Electronic Supplementary Material (ESI) for Inorganic Chemistry Frontiers.

Supporting Information

Design of compressively strained PtRu alloy as anode for high performance DMFC

Shuai Yin[#], Kening Zong[#], Lishou Ban, Huiming Yin [*], Xizheng Liu, Yi Ding

[a] Tianjin Key Laboratory of Advanced Functional Porous Materials, Institute for New Energy Materials & Low-Carbon Technologies, School of Materials Science and Engineering, Tianjin University of Technology, Tianjin 300384, China.

* Corresponding Authors
E-mail address: yinhuiming@tjut.edu.cn

Experimental

1. Materials

Au-Ag alloy film were purchased from Sepp Leaf Products, Inc. Chloroplatinic acid (H_2PtCl_6), ruthenium trichloride ($RuCl_3$), nitric acid (HNO_3), methanol (CH_3OH) and perchloric acid ($HClO_4$) were purchased from Sinopharm Chemical Reagent Co., Ltd. Commercial PtRu/C (Hispec 10000, Pt 40 wt%, Ru 20 wt%) and Pt/C (40 wt%) catalysts were produced by Johnson-Matthey (JM). Nafion resin solution (D-520, 5 wt%) was produced by Dupont. All chemicals in the experiment were used without further purification. All aqueous solutions were prepared using ultrapure water (18.25 MΩ·cm).

Fabrication of electrocatalysts: NPG substrate was fabricated via dealloying method from Au-Ag alloy film in concentrated HNO_3 for 30 min at 30 °C. Electro-deposition of PtRu nanoparticles was carried out using an electrochemical workstation (760D, CHI) with a standard three-electrode system. A graphite plate was used as the counter electrode, and a saturated calomel electrode (SCE) was used as reference electrode. All of the solutions were N_2-saturated before electrochemical measurements. DNPV technique was used to deposit PtRu alloy nanoparticles on NPG substrate. The potential range was set up from 0.3 to -0.2 V and the amplitude was 0.05 V s^{-1}. The Pt/Ru molar ratios of the PtRu alloy nanoparticles were tuned by changing the composition of the plating solutions with H_2PtCl_6, $RuCl_3$ and 0.1 M $HClO_4$. The concentrations of H_2PtCl_6 were fixed to be 2 mM while the concentrations of $RuCl_3$ were modulated with the targeted Pt/Ru molar ratios.

2. Structure Characterization

The crystal phases of all the samples were measured using an X-ray diffraction (XRD) instrument (D/max 2500, Rigaku) with 2θ ranging from 20 to 90° at a scan rate of 5° min^{-1}. The morphology of the samples was obtained by using a high-resolution field emission scanning electron microscope (FESEM, Verios 460L, FEI) equipped with an X-ray energy-dispersive spectrometer (EDS). The compositions of different NPG-PtRu samples were determined by inductively coupled plasma-mass spectrometry (ICP-MS, iCAP RQ, Thermo Fisher) with a dual-channel detector. The atomic

scale surface structure of the samples was obtained using the scanning transmission electron microscopy (STEM) mode of a Titan Cubed Themis G2 300 with a concentrator spherical aberration corrector and Super X spectrometer system. And the HAADF mode was operated at 200 kV. The chemical and electronic states of Au, Pt and Ru were analyzed using X-ray photoelectron spectroscopy (XPS, ESCALAB 250Xi, Thermo Scientific) with a monochromatic Al Kα radiation source.

3. Electrochemical measurements

A glassy carbon electrode (GCE, Φ = 5 mm) coated with the prepared sample was used as working electrode, while a carbon plate and a SCE were used as counter and reference electrodes, respectively. The working electrodes using NPG-PtRu samples were simply prepared by adhering the samples on GCE using Nafion alcohol solution (3 μL, 0.05 wt%) as the glue. The working commercial PtRu/C electrode was fabricated by plating the GCE with uniform catalyst ink of 2 mg PtRu/C, 200 μL Nafion isopropanol solution (0.5 wt%), 400 μL isopropanol and 400 μL ultra-pure water. The coating ink was dried for 30 min at room temperature to form a uniform thin film on the GCE surface. Pt loadings of all the working electrodes were controlled to be ~15 μg cm^{-2}. Typical surface structure of all the catalysts were recorded in N_2-saturated 0.1 M $HClO_4$ solution by using CV between -0.27 and 0.9 V at a scan rate of 50 mV s^{-1}. The MOR activities were measured in N_2-saturated mixture solution of 0.1 M $HClO_4$ and 1 M CH_3OH via CV technique from -0.27 to 0.9 V at a sweeping rate of 50 mV s^{-1}. The electrochemical surface areas (ECSA) and CO-resistance of catalysts were measured by using CO-stripping test. During the CO-stripping test, CO was firstly bubbled into the solution for 20 min. Then the potential of the working electrode was hold at -0.15 V for 10 min via CA technique to make monolayer CO coverage on the electrode surface. After that, the dissolved CO was removed from the solution by bubbling N_2 for 30 min. And the surface adsorbed CO molecules were measured via CV technique with the potentials ranging from -0.27 V to 0.9 V, at a sweeping rate of 20 mV s^{-1}. During the CO-stripping test, CO was firstly bubbled into the solution for 20 min. Then the potential of the working electrode was hold at -0.15 V for 10 min via CA technique to make monolayer CO coverage on the electrode surface. After that, the dissolved CO was removed from the solution by bubbling N_2 for 30 min. And the surface adsorbed

CO molecules were measured via CV technique with the potentials ranging from -0.27 V to 0.9 V, at a sweeping rate of 20 mV s^{-1}. ECSA could be calculated with the equation ECSA = Q_{CO} / (420 μC cm^{-2}) where Q_{CO} is the integral charge of CO oxidation peak. All the experiments were operated at room temperature, and all the electrolytic solutions were purged with high-purity N_2 to remove dissolved O_2 before electrochemical measurements.

4. DFT Calculations

All the geometric optimization and single-point energy calculations were performed using spin-polarized density functional theory (DFT) implemented in the DMol3 code. The Effective Core Potentials (ECP) was the relativistically corrected pseudopotential. The Double Numerial Plus Polarization (DNP) of the p-polarization function was also selected for the calculation of the studied system. The electron exchange and correlation energy were treated within the generalized gradient approximation in the Perdew-Burke-Ernzerhof functional (GGA-PBE).[1,2] The structures used in the calculations were all periodic 4 × 4 cells and each structure had four layers of metal atoms. The bottom layer was immobilized and the other atoms could relax with the adsorbed material. The convergence tolerances of energy, maximum force and displacement were set to 2 × 10^{-5} Ha, 0.004 Ha $Å^{-1}$ and 0.005 Å, respectively. The maximum number of iterations was 1000 and the maximum step size convergence criterion 0.3 Å was employed to ensure high-quality computational results. The self-consistent field (SCF) tolerance was 1 × 10^{-5} eV and a 5 × 5 × 1 Monkhorst-Pack k-point grid was set to optimize the equilibrium lattice constants of unit cells. The number of SCF cycles was 2000 and the (5 × 5 × 1) Monkhorst-Pack k-point grid sampling in the reciprocal space was employed in the calculations.[3] The Gibbs free energy change (ΔG) of the rate-determining step was calculated according to the following formula: $\Delta G = \Delta E_{ads} + \Delta E_{ZPE} - T\Delta S$. Where ΔE_{ads} is the adsorption energy of reaction intermediates; ΔE_{ZPE} and ΔS are the energy difference in zero-point energy and entropy, respectively.[4]

5. Membrane electrode assembly (MEA) construction and testing

Nafion 115 (Dupont) was used as the electrolyte membrane after a sequential treatment in H_2O_2 (3 vol.%), ultra-pure H_2O, H_2SO_4 (0.5 M) and ultra-pure H_2O at 80 °C. Commercial Pt/C was used as

the cathode with a Pt loading of 2 mg cm^{-2}. And a piece of hydrophobic treated carbon paper (TGP-H-060, Toray) sprayed with 1 mg cm^{-2} carbon powder was used as the anodic gas diffusion layer (GDL). NPG-Pt_2Ru_1 anode with Pt loading of 0.21 mg cm^{-2} was prepared by attaching the film on one side of the electrolyte membrane while PtRu/C anode with Pt loading of 2 mg cm^{-2} was fabricated by spraying the ink of PtRu/C and Nafion resin on the anodic GDL. MEAs were constructed by hot-pressing at 130 ^oC for 180 s with a pressure of 75 kg cm^{-2}. In this paper, the MEA using home-made NPG-Pt_2Ru_1 anode is named to be MEA_{home} while that using commercial PtRu/C anode is named to be MEA_{com}. Polarized I-V/I-P curves of these two MEAs were recorded using a fuel cell test system (850e, Scribner). The flow rates of 1 M CH_3OH solution and O_2 were controlled at 1 mL min^{-1} and 200 mL min^{-1}, respectively. Electrochemical impedance spectra (EIS) were measured with a potentiostat (IM6, Zahner) with an amplitude of 10 mV from 0.1 Hz to 100 kHz. And the fuel cell was operated at a current density of 100 mA cm^{-2} with an anodic feed of 1 M methanol solution. Stability tests were obtained by operating the MEAs at a constant current density of 100 mA cm^{-2}. The amount of methanol crossing from anode side to cathode side was measured referring to previous literatures.[5] The anode, fed with methanol solution (1.0 M) at 1 mL min^{-1} was used as the reference and counter electrodes. And the cathode, fed with N_2 at a flow rate of 50 ml min^{-1} was used as the working electrode. Under these conditions, positive scanning linear sweep voltammetry (LSV) curves were recorded from 0.2 V at a sweeping rate of 2 mV s^{-1}. The obtained oxidation peak was mainly ascribed to methanol oxidation reaction in the cathode side and therefore the current densities could be used to compare methanol amounts crossed from the anode sides. The anodic CV measurements of MEA were tested according to the previous reported protocol,[6] which was performed to measure the structural stability of the anode catalyst layer before and after durability tests. The cathode side was fed with hydrogen with a flow rate of 50 SCCM (considered as a dynamic hydrogen electrode (DHE)) as both reference and counter electrode, while the anode side was fed with DI water with a flow rate of 1 mL min^{-1} as the working electrode. CV curves were measured by scanning the potential anode electrode at a scanning rate of 20 mV s^{-1} from 0 to 1.2 V.

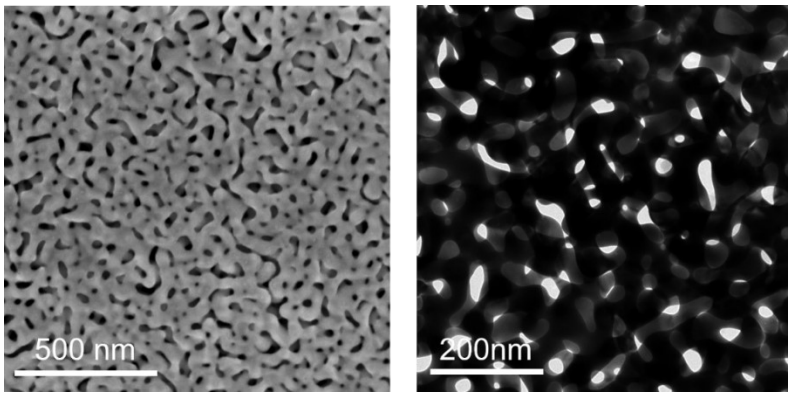

Fig. S1. Low magnification SEM and TEM images of NPG.

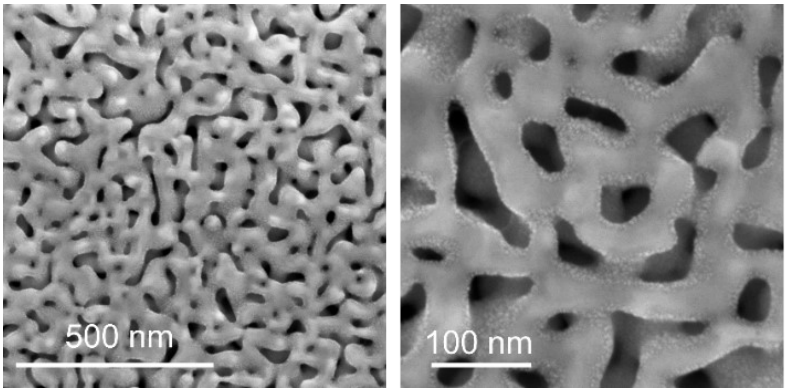

Fig. S2. SEM images with varied magnifications of NPG-Pt_2Ru_1 sample.

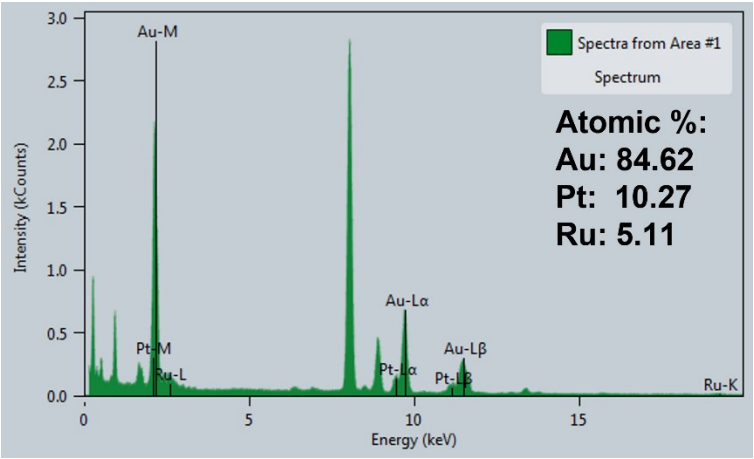

Fig. S3. EDS spectrum of NPG-Pt_2Ru_1 sample.

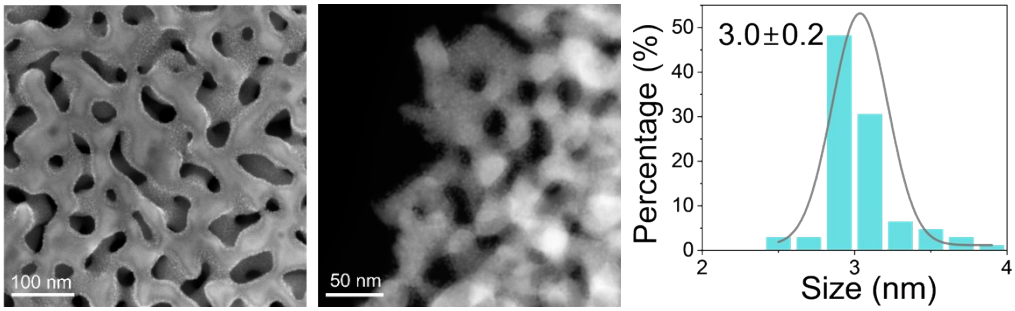

Fig. S4. SEM images with varied magnifications and nanoparticle size distribution chart of NPG-Pt_1Ru_1 sample.

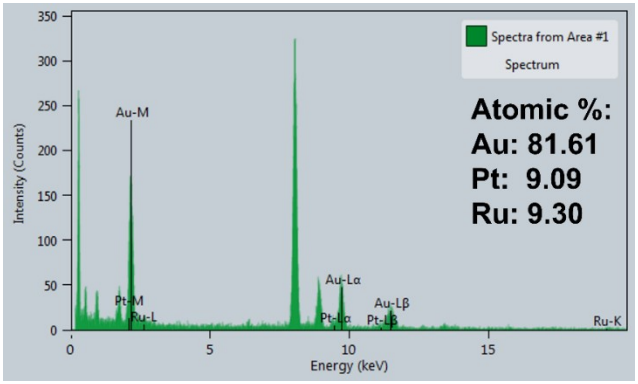

Fig. S5. EDS spectrum of NPG-Pt_1Ru_1 sample.

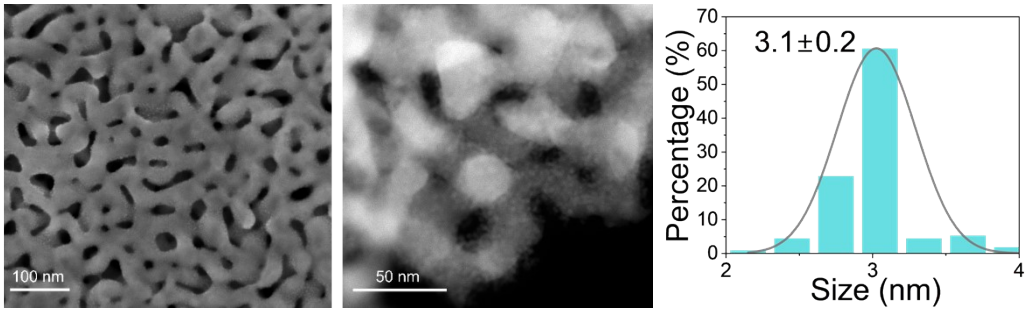

Fig. S6. SEM images with varied magnifications and nanoparticle size distribution chart of NPG-Pt_1Ru_2 sample.

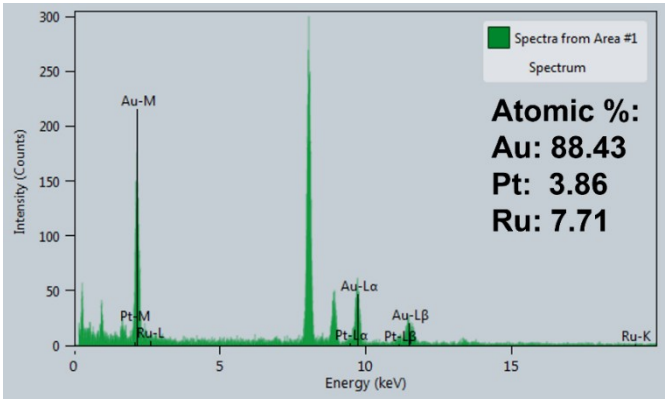

Fig. S7. EDS spectrum of nanoporous NPG-Pt_1Ru_2 alloy.

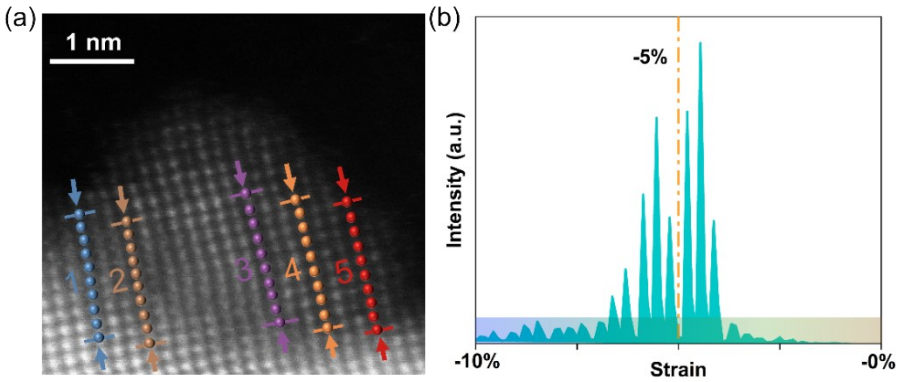

Fig. S8. (a) Enlarged HAADF-STEM image of the yellow square marked in Fig. 1f. (b) Histogram of strain distribution of NPG-Pt_2Ru_1 obtained at the center site.

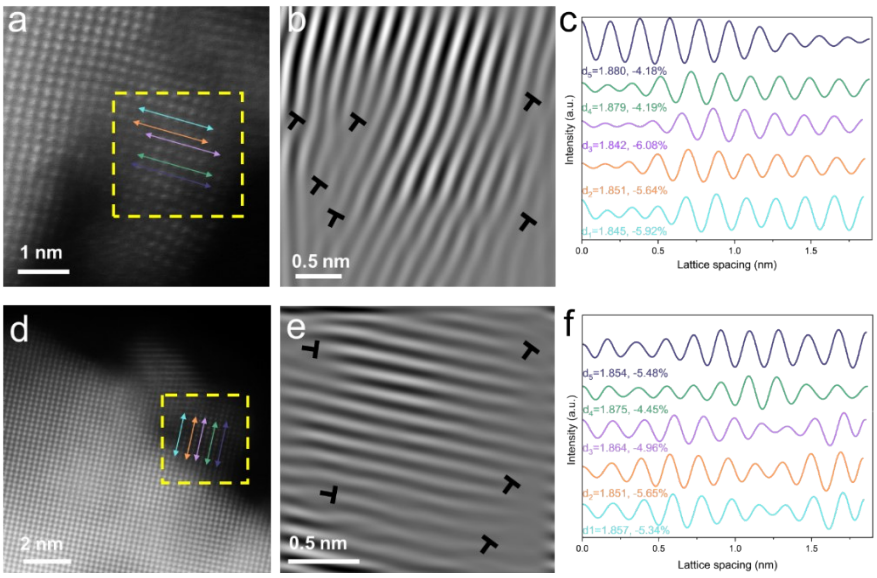

Fig. S9. Atomic resolution HAADF images and corresponding iFFT patterns of (200) plane, intensity profiles of lattice spacing of selected regions (yellow dashed rectangles) observed from NPG-Pt_1Ru_1(a-c) and NPG-Pt_1Ru_2(d-f).

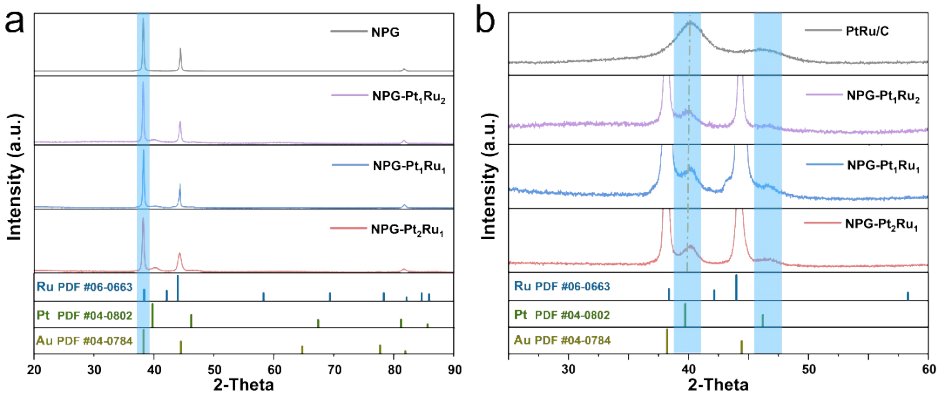

Fig. S10. (a) XRD patterns in the full 2θ range of 20° to 90°compared with NPG-Pt_2Ru_1, NPG-Pt_1Ru_1, NPG-Pt_1Ru_2, and NPG. PDF cards of Au (JCPDS: 04-0784, brown), Pt (JCPDS: 04-0802, green) and Ru (JCPDS: 06-0663, azury) are as illustrated below the XRD patterns. (b) Regional enlarged drawing and compared with PtRu/C.

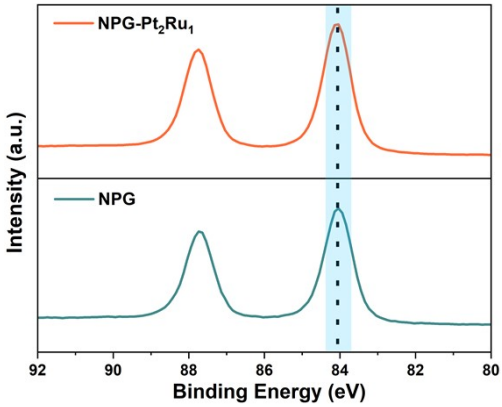

Fig. S11. XPS spectra of NPG and NPG-Pt_2Ru_1.

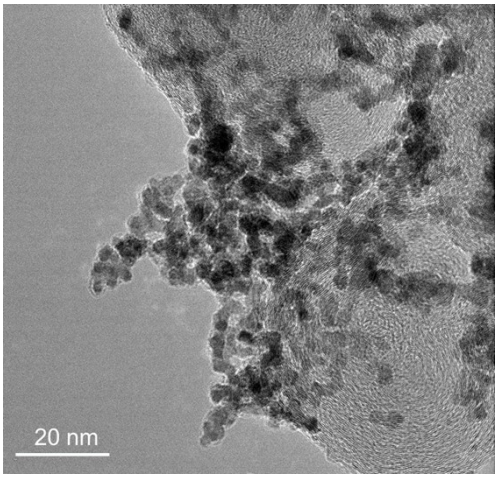

Fig. S12. TEM image of commercial PtRu/C.

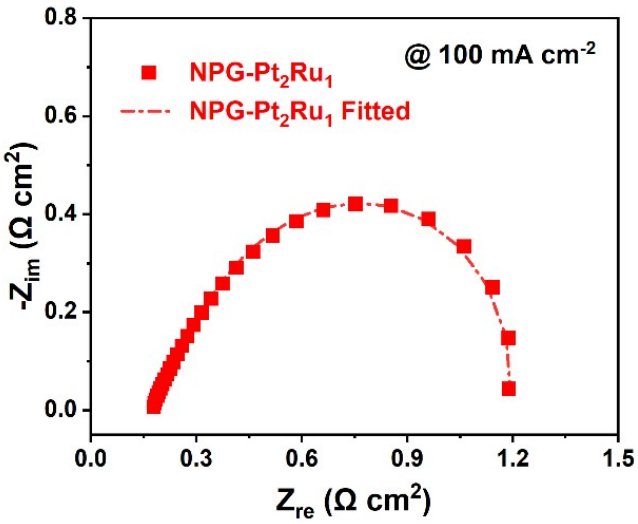

Fig. S13. EIS spectra at 100 mA cm^{-2}.

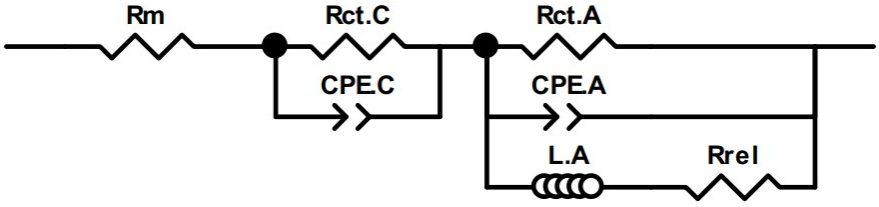

Fig. S14. The equivalent circuit diagram of the DMFC single cell.

Table S1. ICP-MS data of NPG-PtRu samples.

Sample	Pt (at.%)	Ru (at.%)	Au (at.%)
NPG-Pt_2Ru_1	17.80	8.70	73.50
NPG-Pt_1Ru_1	15.96	16.30	67.74
NPG-Pt_1Ru_2	12.67	25.35	61.68

Table S2. A comparison of MOR activities for different electrocatalysts.

Sample	ECSA ($m^2\ g^{-1}$)	Electrochemical area (cm^2)	SA (mA cm^{-2})	MA (A mg^{-1})
NPG-Pt_2Ru_1	86.9	2.56	1.888	1.642
NPG-Pt_1Ru_1	83.3	2.45	1.469	1.224
NPG-Pt_1Ru_2	72.4	2.13	1.465	1.061
PtRu/C	58.6	1.73	0.722	0.423
Pt/C	67.6	1.98	0.521	0.352

Table S2. Electrochemical performances for different kinds of Pt-based nanocatalysts for methanol oxidation

Materials	Mass activity	Specific activity	Electrolyte	Ref.
NPG-Pt_2Ru_1	1.64 A mg_{Pt}^{-1}	1.89 mA cm_{Pt}^{-2}	0.1 M $HClO_4$ 1.0 M CH_3OH	This work
d-Pt@Ru dodecahedra	0.8 A mg_{Pt}^{-1}	1.61 mA cm_{Pt}^{-2}	0.5 M H_2SO_4 1.0 M CH_3OH	[7]
PtRu nanowires	0.82 A mg_{Pt}^{-1}	1.16 mA cm_{Pt}^{-2}	0.1 M $HClO_4$ 0.5 M CH_3OH	[8]
PtRu dilute alloy nanodendrites	1.14 A mg_{Pt}^{-1}	2.66 mA cm_{Pt}^{-2}	0.1 M $HClO_4$ 0.5 M CH_3OH	[9]
Ru@$Pt_{0.5}$/C	1.3138 A mg_{Pt}^{-1}	~	0.5 M H_2SO_4 1.0 M CH_3OH	[10]
PtRuCu/C	1.35 A mg_{Pt}^{-1}	3.92 mA cm_{Pt}^{-2}	0.1 M $HClO_4$ 1.0 M CH_3OH	[11]
PtRu/rGO-2	739 mA mg_{Pt}^{-1}	1.067 mA cm_{Pt}^{-2}	0.5 M H_2SO_4 1.0 M CH_3OH	[12]
Pt/RuO_2/G	841.9 mA mg_{Pt}^{-1}	~	1.0 M H_2SO_4 2.0 M CH_3OH	[13]
Pt_1Ru_3 nano-sponge	410 mA mg_{Pt}^{-1}	~	0.5 M H_2SO_4 1.0 M CH_3OH	[14]
PtCuRu	678 mA mg_{Pt}^{-1}	2.31 mA cm_{Pt}^{-2}	0.5 M H_2SO_4 1.0 M CH_3OH	[15]

Table S3. The comparison of MEA performance according to different literatures.

Samples	C_{MeOH}/M	T/°C	PtRu loading (mg cm^{-2})	Mass activity (mW mg_{pt}^{-1})	Area activity (mW cm^{-2})	Ref.
PtRu-CoP/C-40%	2	70	2	64	128	[16]
PtRu/NCNT-GHN	2	90	7	27.9	195.1	[17]
Pt-Ru/BDDNP	1	80	4	13.8	55	[18]
PtRu Black-JM	2	55	4	5	20.1	[19]
PtRu/C-JM	2	65	2.5	13.2	33	[20]
PtRu alloy	2	70	3	54	162	[21]
PtRu/TECNF	2	80	0.58	84.5	49	[22]
PANI/PtRu/C	2	80	4	24	96	[23]
PtRu/C-SA	1	80	7.5	14.7	110	[24]
PtRu/ordered porous carbons	2	30	3	19.3	58	[25]
PtRu/C (20%:15%)	2	80	3	26	78	[26]
PtRu black (1:1)	2	90	2	90	180	[27]
NPG-Pt_2Ru_1	1	80	0.264	557.1	117	This work

Table S4. Fitting parameters for the equivalent circuit model for all the MEAs in 1 M methanol concentrations.

	Catalyst	Rm (Ω cm^2)	Rct.C (Ω cm^2)	CPE.C-T (F cm^{-2})	CPE.C-P	Rct.A (Ω cm^2)	CPE.A-T (F cm^{-2})	CPE.A-P	Rrel (Ω cm^2)	LA (H cm^{-2})
1 M, 80 ℃	PtRu/C	0.187	0.685	0.012	0.739	0.711	0.018	0.737	0.185	0.015
	PtRu/C 18 h	0.193	0.764	0.007	1.006	0.811	0.013	0.701	0.182	0.018
	NPG-Pt_2Ru_1	0.171	0.592	0.004	1.002	0.565	0.016	0.688	0.171	0.011
	NPG-Pt_2Ru_1 18 h	0.175	0.645	0.004	1.038	0.596	0.015	0.659	0.184	0.012

Reference

[1] G. Kresse, J. Furthmüller, Efficient iterative schemes for ab initio total-energy calculations using a plane-wave basis set, *Physical Review B* **1996**, *54*, 11169-11186.

[2] J.P. Perdew, K. Burke, M. Ernzerhof, Generalized gradient approximation made simple, Physical Review Letters **1996**, *77*, 3865-3868.

[3] H.J. Monkhorst, J.D. Pack, Special points for Brillouin-zone integrations, *Physical Review B*, **1976**, *13*, 5188-5192.

[4] J.K. Nørskov, J. Rossmeisl, A. Logadottir, L. Lindqvist, J.R. Kitchin, T. Bligaard, H. Jónsson, Origin of the overpotential for oxygen reduction at a fuel-cell cathode, *Journal of Physical Chemistry B* **2004**, *108*, 17886-17892.

[5] S. Jang, S. Kim, S.M. Kim, J. Choi, J. Yeon, K. Bang, C.-Y. Ahn, W. Hwang, M. Her, Y.-H. Cho, Y.-E. Sung, M. Choi, Interface engineering for high-performance direct methanol fuel cells using multiscale patterned membranes and guided metal cracked layers, *Nano Energy* **2018**, *43*, 149-158.

[6] F. Jing, R. Sun, S. Wang, Y. Li, C. Yang, W. Ma, H. Sun, G. Sun, Influencing factors on the stability of direct methanol fuel cells, *Fuel Cells* **2019**, *19*, 731-739.

[7] X. Bai, J. Geng, S. Zhao, H. Li, F. Li, *ACS Applied Materials & Interfaces* **2020**, *12*, 23046.

[8] L. Huang, X. Zhang, Q. Wang, Y. Han, Y. Fang, S. Dong, *Journal of the American Chemical Society* **2018**, *140*, 1142.

[9] S. Zhang, H. Rong, T. Yang, B. Bai, J. Zhang, *Chemistry – A European Journal* **2020**, *26*, 4025.

[10] J. Xie, Q. Zhang, L. Gu, S. Xu, P. Wang, J. Liu, Y. Ding, Y. F. Yao, C. Nan, M. Zhao, Y. You, Z. Zou, *Nano Energy* **2016**, *21*, 247.

[11] S. Xue, W. Deng, F. Yang, J. Yang, I. S. Amiinu, D. He, H. Tang, S. Mu, *ACS Catalysis* **2018**, *8*, 7578.

[12] Y. Shi, W. Zhu, H. Shi, F. Liao, Z. Fan, M. Shao, *Journal of Colloid and Interface Science* **2019**, *557*, 729.

[13] H. Huang, J. Zhu, D. Li, C. Shen, M. Li, X. Zhang, Q. Jiang, J. Zhang, Y. Wu, *Journal of Materials Chemistry A* **2017**, *5*, 4560.

[14] M. Xiao, L. Feng, J. Zhu, C. Liu, W. Xing, *Nanoscale* **2015**, *7*, 9467.

[15] L. Bai, S. Li, L. Fang, Z. Chen, Z. Li, *Langmuir* **2020**, *36*, 7602.

[17] L. Feng, K. Li, J. Chang, C. Liu, W. Xing, *Nano Energy* **2015**, *15*, 462.

[17] R. Lv, T. Cui, M.-S. Jun, Q. Zhang, A. Cao, D. S. Su, Z. Zhang, S.-H. Yoon, J. Miyawaki, I. Mochida, F. Kang, *Advanced Functional Materials* **2011**, *21*, 999.

[18] L. La-Torre-Riveros, R. Guzman-Blas, A. E. Méndez-Torres, M. Prelas, D. A. Tryk, C. R. Cabrera, *ACS Applied Materials & Interfaces* **2012**, *4*, 1134.

[19] Y. Wang, G. Liu, M. Wang, G. Liu, J. Li, X. Wang, *International Journal of Hydrogen Energy* **2013**, *38*, 9000.

[20] Z. Jiang, Y. Shi, Z.-J. Jiang, X. Tian, L. Luo, W. Chen, *Journal of Materials Chemistry A* **2014**, *2*, 6494.

[21] S.-A. Lee, K.-W. Park, J.-H. Choi, B.-K. Kwon, Y.-E. Sung, *Journal of The*

Electrochemical Society **2002**, *149*, A1299.
[22] Y. Ito, T. Takeuchi, T. Tsujiguchi, M. A. Abdelkareem, N. Nakagawa, *Journal of Power Sources* **2013**, *242*, 280.
[23] M. Zhiani, H. Gharibi, K. Kakaei, *Journal of Power Sources* **2012**, *210*, 42.
[24] M. Carmo, M. Brandalise, A. O. Neto, E. V. Spinacé, A. D. Taylor, M. Linardi, J. G. Rocha Poço, *International Journal of Hydrogen Energy* **2011**, *36*, 14659.
[25] G. S. Chai, S. B. Yoon, J.-S. Yu, J.-H. Choi, Y.-E. Sung, *The Journal of Physical Chemistry B* **2004**, *108*, 7074.
[26] W. Xu, T. Lu, C. Liu, W. Xing, *The Journal of Physical Chemistry B* **2005**, *109*, 14325.
[27] D. Sebastián, V. Baglio, A. S. Aricò, A. Serov, P. Atanassov, *Applied Catalysis B: Environmental* **2016**, *182*, 297.